Nano Research 2013, 6(2): 131–137
DOI 10.1007/s12274-013-0288-8
Research Article
ISSN 1998-0124
CN 11-5974/O4

Template-directed assembly of pentacene molecules on epitaxial graphene on Ru(0001)

Haitao Zhou[1], Lizhi Zhang[1], Jinhai Mao[1], Geng Li[1], Yi Zhang[1], Yeliang Wang[1], Shixuan Du[1] (✉), Werner A. Hofer[2], and Hong-Jun Gao[1] (✉)

[1] *Institute of Physics, Chinese Academy of Sciences, Beijing 100190, China*
[2] *Stephenson Institute for Renewable Energy, University of Liverpool, Liverpool L69 3BX, UK*

Received: 18 October 2012
Accepted: 20 December 2012

KEYWORDS
graphene, Ru(0001), pentacene, self-assembly, scanning tunneling microscopy (STM), density functional theory (DFT)

ABSTRACT

The template-directed assembly of planar pentacene molecules on epitaxial graphene grown on Ru(0001) (G/Ru) has been investigated by means of low-temperature scanning tunneling microscopy (STM) and density functional theory (DFT) calculations. STM experiments find that pentacene adopts a highly selective and dispersed growth mode in the initial stage. By using DFT calculations including van der Waals interactions, we find that the configuration with pentacene adsorbed on face-centered cubic (fcc) regions of G/Ru is the most stable one, which accounts for the selective adsorption at low coverage. Moreover, at high coverage, we have successfully controlled the molecular assembly from amorphous, local ordering, to long-range order by optimizing the deposition rate and substrate temperature.

1 Introduction

Graphene has attracted great attention due to its unique electronic properties and potential applications [1]. Many methods for fabricating graphene have been proposed, such as mechanical exfoliation [2], or epitaxial growth on metals [3–5] and SiC [6, 7]. Among these approaches, graphene grown on Ru(0001) is very promising because of the ease of fabrication and the large, continuous samples obtained—both are of great importance for future electronic devices. Much work has also been focused on organic molecule adsorption on graphene/Ru(0001) (G/Ru) [8–12] and analogous substrates (such as G/Ir and G/SiC) [13–16]. The increasing interest in such structures is due to several aspects. First, graphene grown on metal substrates with a lattice mismatch always forms a regular moiré pattern. The impact of this superstructure on the adsorption behavior and lateral ordering of organic molecules is fundamentally interesting and important, but little is known so far. Moreover, in technological applications graphene must be combined with other

Address correspondence to Shixuan Du, sxdu@iphy.ac.cn; Hongjun Gao, hjgao@iphy.ac.cn

materials to manufacture actual devices. Among the many candidate substances for nanoelectronic devices, organic molecules are an obvious choice due to their large range of functional properties. Graphene-based organic solar cells have already been fabricated and analyzed [17, 18] and it is also known that charge-carrier mobility in organic devices depends significantly on molecular orientation and packing [19]. In view of these applications it is desirable to improve control during the initial growth process.

In this work, the adsorption behavior of pentacene molecules on G/Ru was investigated combining scanning tunneling microscopy (STM) experiments and density functional theory (DFT) calculations. Pentacene was chosen due to its wide use both in research on molecular self-organization [20–23] and in the design of photovoltaic cells where it acts as donor [24, 25]. Unlike prior studies of molecule–graphene interfaces such as perylene-3,4,9,10-tetracarboxylic dianhydride (PTCDA)–G/SiC [13], (2,3,5,6-tetrafluoro)-7,7,8,8-tetracyano-p-quinodimethane ($(F_4$-)TCNQ)–G/Ir [15], C_{60}–G/Ru [11], and FePc–G/Ru [10], which merely focused on a particular dosage, we systematically investigated progressive growth behavior at a wide range of coverages. The selective and dispersed adsorption of pentacene on G/Ru in the initial stage was due to the adsorption energy differences of pentacene on G/Ru with different adsorption sites. We then successfully controlled the growth of a single molecular layer with structures ranging from amorphous to fully ordered by controlling the deposition rate and substrate temperature.

2 Experimental and calculation details

The experiments were performed with a commercial Omicron low temperature STM system with a base pressure better than 1×10^{-10} mbar. The atomically flat Ru(0001) surface was prepared by cycles of argon-ion sputtering and high temperature annealing. Graphene was formed on this surface by exposing the ruthenium substrate to ethylene at 1,300 K and a pressure of 1×10^{-6} mbar for about 3 min. Pentacene (Sigma, 99+%) was carefully purified by temperature gradient sublimation and then thermally evaporated onto graphene. Several deposition conditions (different evaporator and/or substrate temperatures, see the Electronic Supplementary Material (ESM)) were used to alter the structures of the pentacene layer. Subsequently, the samples were cooled down to 5 K for STM imaging. In every case, the voltage was applied to the sample with respect to the tip.

To gain insight into the growth mechanism of pentacene molecules on G/Ru, we have carried out theoretical calculations. The calculations were based on DFT, as implemented in the Vienna *ab initio* simulation package (VASP) [26, 27]. Projector augmented wave potentials were used to describe the core electrons and a generalized gradient approximation of Perdew, Burke, and Ernzernhof (PBE) to describe exchange and correlation [28]. Since van der Waals (vdW) forces provide the main interaction between pentacene and the G/Ru, and as the vdW or dispersion force often plays a crucial role in the adsorption of aromatic molecules, we used Grimme corrections to take into account the vdW forces [29]. The parameters in our DFT + D/PBE calculations are described elsewhere [30]. The periodic slab model included three layers of Ru(0001), one layer of graphene, one pentacene molecule and a vacuum layer of 15 Å. A moiré unit cell with 12 × 12 graphene on 11 × 11 Ru(0001) was used. All atoms were fully relaxed except for the bottom two substrate layers, until the net force on every atom was less than 0.02 eV/Å. In our calculations, the energy cutoff of the plane-wave basis sets was 400 eV, and, due to numerical limitations, only the Γ point was employed for Brillouin zone integrations.

3 Results and discussion

A graphene monolayer on Ru(0001) forms a well aligned hexagonal moiré pattern, originating from the lattice mismatch between graphene and Ru(0001). This superstructure has a periodicity of 30 Å and an apparent corrugation of about 1 Å. Figure 1(a) is a high resolution, atomically resolved STM image of the moiré topography with the unit cell outlined by a rhombus. Three regions can be unambiguously distinguished in this unit cell: The bright region (marked by a solid circle), the intermediate region (marked by a solid triangle) and the dark region (marked by a dashed triangle), which are assigned to the atop, face-centered

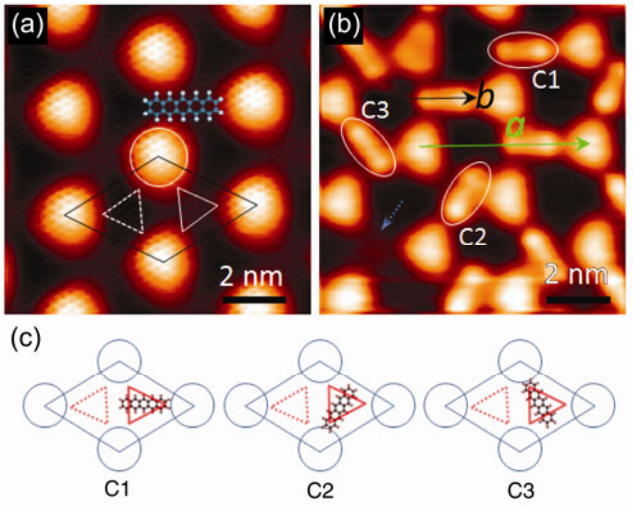

Figure 1 STM images and schematics of pentacene on G/Ru at low coverage. (a) STM atomic-resolution image of graphene on Ru(0001) with a rhombus indicating the moiré unit cell. Three distinct areas in a unit cell are outlined by solid circle (atop), solid triangle (fcc), and dashed triangle (hcp), respectively, with a model of pentacene. (b) STM image showing pentacene molecules preferentially adsorbed on fcc regions. The ellipses indicate the three configurations. Vectors ***a*** and ***b*** are used to indicate the atop-atop direction of G/Ru and the long symmetric axis of pentacene, respectively. (c) Schematic illustration of the three equivalent adsorption configurations. Rhombus and circle indicate the moiré unit cell and atop site, respectively. Scanning parameters: (a) V_s = –0.02 V, I = 4.0 nA, (b) V_s = –2.0 V, I = 0.09 nA.

cubic (fcc) and hexagonal close packed (hcp) regions, respectively. Each region represents different arrangements of the carbon honeycomb pattern with respect to the underlying ruthenium substrate [10, 31].

Linear-shaped pentacene molecules are deposited onto this corrugated template. As seen in Fig. 1(b), pentacene adopts a dispersed and highly selective adsorption mode at low coverage (< 0.1 monolayer (ML)), indicating that the growth of pentacene is strongly mediated by the moiré structure. However, on a highly oriented pyrolytic graphite (HOPG) surface, pentacene tends to aggregate into islands due to the minimal variation in adsorption potential [32]. With the aid of an unoccupied fcc region marked by a dashed arrow in the lower left of Fig. 1(b), we can conclude that molecules preferentially adsorb on the fcc region of the moiré template. Further inspection shows that pentacene molecules exhibit three possible adsorption configurations, labeled as C1, C2, and C3 in Fig. 1(b). All three of these configurations are oriented toward atop regions, but are rotated with respect to each other. We find that the three molecular orientations (***b***) are 0° ± 2°, 60° ± 2°, and 120° ± 2° relative to the substrate axis (***a***) (the error bars are estimated by a statistical averaging of several STM images). The three angles align well with the three-fold symmetry of the fcc region, hence C1, C2, and C3 are equivalent configurations. The three molecular configurations as well as graphene unit cells are schematically represented in Fig. 1(c).

As we increase the coverage, pentacene molecules first occupy all the fcc regions and subsequently start to reside on hcp regions. In the following, we refer to molecules on fcc (hcp) sites as fcc (hcp)-molecules. In Fig. 2(a), four rhombuses outline moiré unit cells whose hcp regions are occupied by molecules. Note that a few of fcc sites are occupied by multiple molecules rather than single molecule, as pointed out by arrows in Fig. 2(a). However, the probability of this phenomenon is less than 1% in our statistical analysis. This is consistent with our conclusion that pentacene prefers to occupy fcc site with single molecule. We lean to attribute this phenomenon to the defects of the moiré pattern, which change the local adsorption energy for molecules (see Fig. S1 in the ESM). For hcp adsorption, in most case molecules form parallel ordered clusters (they sometimes also form disordered clusters, see Fig. S2 in the ESM). Two enlarged STM images of such clusters are displayed

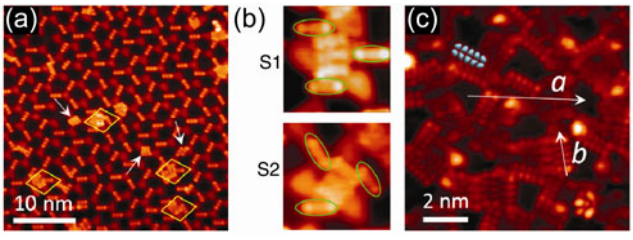

Figure 2 STM images of pentacene on G/Ru at high coverages. (a) Pentacene molecules sequentially adsorb on hcp regions after occupying all fcc sites. (b) Zoom-in STM images showing two typical adsorption scenarios (S1 and S2) of hcp-molecules. The fcc-molecules are indicated by ellipses and hcp-molecules lie in parallel in between. (c) Molecules occupy all fcc and hcp regions, leaving the atop regions unoccupied. A calculated highest occupied molecular orbital (HOMO) is superimposed to facilitate identification of pentacene molecules. Vectors ***a*** and ***b*** are used to highlight the orientations of molecules. Scanning parameters: (a) V_s = –3.0 V, I = 0.05 nA, (b) and (c) V_s = –2.0 V, I = 0.1 nA.

in Fig. 2(b). In each image, ellipses highlight three fcc-molecules. The hcp region surrounded by these fcc-molecules is occupied by three parallel hcp-molecules. However, there are two distinct scenarios (S1 and S2) for hcp-molecules regarding their relative orientations with respect to surrounding fcc-molecules. In the upper panel, the orientation of hcp-molecules nearly coincides with that of neighboring fcc-molecules—a case we refer to as scenario S1. In the lower panel, hcp-molecules are not parallel to any of the three adjacent fcc-molecules—a case referred to as scenario S2. Note that in S1 the orientation of an hcp-molecule can be any of the three values (0°, 60°, and 120°) corresponding to the three initial fcc-molecular configurations (C1, C2, and C3).

With further dosing, pentacene will occupy almost all fcc and hcp regions and leave atop regions unoccupied, as shown in Fig. 2(c). In this image, the dark holes are the locations of the unoccupied atop regions. Strictly, some molecules have crossed the boundaries between fcc/hcp and atop regions due to the high coverage. However, it is obvious that the majority of the atop region is unoccupied, indicating it is less preferable for molecular adsorption. Individual pentacene molecules display a ten-lobe rod-like shape, which is identical to the calculated highest occupied molecular orbital (HOMO) of a free molecule, owing to the weak electronic hybridization at the molecule-graphene interface [33]. Pentacene forms a disordered sub-layer at this coverage (~0.7 ML), featuring some localized parallel-packed molecular clusters evolved from the adsorption scenario discussed in Fig. 2(b).

We calculated the adsorption energy for eight possible adsorption configurations labeled as fcc-R0, fcc-R30, hcp-R0, hcp-R30, atop-R0, atop-R30, fcc-2-R0, and fcc-2-R30, as shown in Fig. 3. Fcc-R0, hcp-R0, and atop-R0 denote one pentacene molecule adsorbed on the fcc, hcp, and atop regions of G/Ru with the same molecular orientation as shown in Fig. 1(b), respectively. Fcc-R30, hcp-R30 and atop-R30 denote the identical adsorption sites, but with a 30° rotation of the pentacene molecules. Fcc-2-R0 (fcc-2-R30) refers to two pentacene molecules adsorbed on the fcc region of G/Ru with the same orientation as fcc-R0 (fcc-R30). The configurations with 30° rotation of the molecule compared to the molecules shown in Fig. 1(b) are

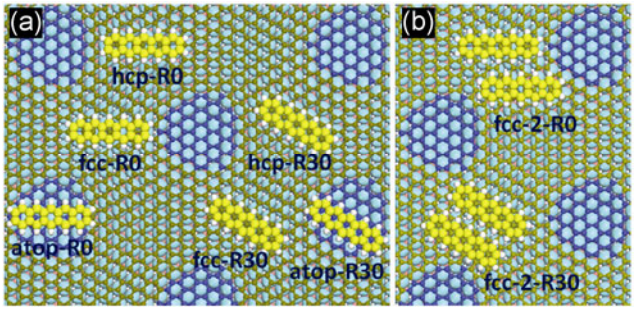

Figure 3 Schematic configurations of pentacene adsorbed on G/Ru. (a) Six configurations for single molecular adsorption denoted as fcc-R0, hcp-R0, atop-R0, fcc-R30, hcp-R30, and atop-R30. (b) Two configurations for parallel adsorption of two pentacene molecules denoted as fcc-2-R0 and fcc-2-R30.

modeled, because they are frequently in evidence in Fig. 2(c) (see Table S1 in the ESM). Table 1 shows the calculated adsorption energy per molecule for each configuration displayed in Fig. 3. Calculations unambiguously confirm that the fcc-R0 molecule has the highest adsorption energy and that it is the most stable configuration among the configurations calculated. This implies that pentacene molecules prefer the fcc region to the hcp and atop regions of G/Ru, which is in good agreement with our experimental observations of the selective adsorption of pentacene on the fcc region. Moreover, our calculation results clearly point out that a configuration with two molecules in the same region is less stable than a configuration with a single molecule. This agrees well with the experimental finding that pentacene molecules adsorb dispersedly on G/Ru at low coverage.

The pentacene molecules form disordered structures at high molecular coverage (~0.7 ML, see Fig. 2(c)). In order to obtain ordered self-assembled structures we investigated the influence of substrate temperature and deposition rate on the structure and morphology of pentacene film [34]. As shown in Fig. 4(a), a short-range ordered pattern is formed at much higher substrate temperature (T_s = 60 ˚C) due to the greater thermally activated surface diffusion. The molecular ordering can be confined within regions measuring tens of nanometers; this gives rise to a large number of small ordered domains as outlined by dashed irregular polygons. A typical domain, shown in an enlarged STM topography (inset of Fig. 4(a)) is formed by five pentacene molecules in short side-by-side chains on

Table 1 Adsorption energies per molecule for the eight adsorption configurations calculated by using DFT based calculations including vdW interactions

Configuration	fcc-R0	fcc-R30	hcp-R0	hcp-R30	atop-R0	atop-R30	fcc-2-R0	fcc-2-R30
Adsorption energy (eV)	2.636	2.612	2.507	2.503	1.820	1.880	2.496	2.407

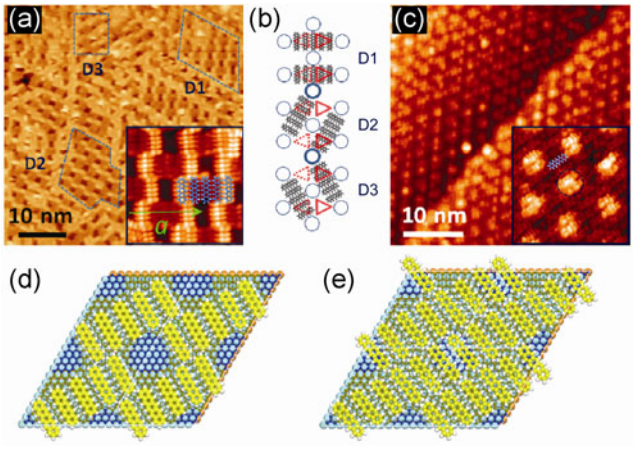

Figure 4 STM images and schematic illustrations of pentacene molecules on G/Ru with short- and long-range ordered structure. (a) STM image indicating that molecular ordering can be confined within regions measuring tens of nanometers. Three domains are outlined by dashed lines and denoted as D1, D2, and D3. The inset is an enlarged STM image (7.5 nm × 7.5 nm), showing a domain with molecular models superimposed to guide the eye and a vector ***a*** marking the atop–atop direction of graphene. (b) Schematic representations show the three basic molecular orientations of the domains in (a). (c) STM image of a uniform pentacene layer and zoom-in image showing side-by-side long-range ordering, with bright protrusions (outlined by dashed circle) due to the structural influence of underlying graphene moiré pattern on pentacene film. (d) and (e) Theoretical models of the loose- and close-packed structure, with an *adsorption energy per area* of 1.49 eV/nm^2 and 1.80 eV/nm^2, respectively. Scanning parameters: (a) V_s = –2 V, I = 0.05 nA, for inset is the same. (c) V_s = –2.0 V, I = 0.05 nA, for inset, V_s = 2.0 V, I = 0.05 nA.

both fcc and hcp regions, leaving the atop region empty. Further investigations show that these domains have only three orientations, denoted as D1, D2, and D3 in Fig. 4(a), which are schematically represented in Fig. 4(b). The three basic constituents are energetically equivalent due to the three-fold symmetry of the moiré template. Thus, a random mixture of the three constituents gives rise to the construction of a locally-ordered pentacene film. As we increase the temperature further to T_s = 90 ℃ and T_e = 180 ℃ (corresponding to a deposition rate of ~0.25 ML/min, six times higher than that in Fig. 2(c)), molecules self-assemble into a uniform film with long-range ordering and close-packed structure, as displayed in Fig. 4(c). We ascribe the formation of this homogeneous pattern to a combination of desorption and diffusion processes. Our experiments prove that loose-packed pentacene films, as shown in Fig. 2(c) and 4(a), will completely be desorbed at substrate temperatures above ~75 ℃ due to the weak interactions at the molecule–graphene interface. However, when molecules assemble into a close-packed pattern, intermolecular interactions will make the film more stable. These films could only be desorbed at a higher temperature. To clarify this point, we also carried out DFT calculations based on the models shown in Fig. 4(d) and 4(e), which are constructed to mimic the STM topography of the Fig. 4(a) and 4(c). Theoretical results explicitly show that the close-packed structure has an *adsorption energy per area* 20.8% higher than the loose-packed one, demonstrating that the former is more stable. Here we consider *adsorption energy per area* rather than *adsorption energy per molecule* due to different molecular densities of the two self-assembled patterns [35, 36]. Hence, we conclude that under these deposition conditions, molecules tend to aggregate into close-packed islands, otherwise they will totally be desorbed from the graphene surface.

4 Conclusions

We have demonstrated that the corrugated moiré structure of a graphene/Ru(0001) interface significantly modulates the growth behavior of pentacene. Molecules preferentially reside on fcc regions with three equivalent configurations, and subsequently occupy hcp regions mainly involving two adsorption scenarios. DFT calculations show that the dispersed and selective adsorption behavior of pentacene on G/Ru at low coverage is controlled by the adsorption energy of

molecules on the substrate. Moreover, by controlling the deposition rate and substrate temperature, the self-assembled structure changes from disorder, local order to long-range order.

Acknowledgements

This work was financially supported by the Ministry of Science and Technology (MOST Nos. 2011CB921702 and 2011CB932700), National Natural Science Foundation of China (NSFC No. 61222112), Multilevel Molecular Assemblies: Structure, Dynamics, and Functions (TRR61), Shanghai Supercomputer Center (SSC), and Chinese Academy of Sciences (CAS) in China. WAH acknowledges support from the UK Car-Parinello consortium, grant No. EP/F037783/1.

Electronic Supplementary Material: Supplementary material (details of defects giving rise to the multiple adsorption on fcc, hcp-adsorption of molecules, orientation statistics, and deposition conditions) is available in the online version of this article at http://dx.doi.org/10.1007/s12274-013-0288-8.

References

[1] Geim, A. K.; Novoselov, K. S. The rise of graphene. *Nat. Mater.* **2007**, *6*, 183–191.

[2] Novoselov, K. S.; Geim, A. K.; Morozov, S. V.; Jiang, D.; Zhang, Y.; Dubonos, S. V.; Grigorieva, I. V.; Firsov, A. A. Electric field effect in atomically thin carbon films. *Science* **2004**, *306*, 666–669.

[3] Pan, Y.; Zhang, H. G.; Shi, D. X.; Sun, J. T.; Du, S. X.; Liu, F.; Gao, H. J. Highly ordered, millimeter-scale, continuous, single-crystalline graphene monolayer formed on Ru(0001). *Adv. Mater.* **2009**, *21*, 2777–2780.

[4] N'Diaye, A. T.; Bleikamp, S.; Feibelman, P. J.; Michely, T. Two-dimensional Ir cluster lattice on a graphene moire on Ir(111). *Phys. Rev. Lett.* **2006**, *97*, 215501.

[5] Li, X. S.; Cai, W. W.; An, J. H.; Kim, S.; Nah, J.; Yang, D. X.; Piner, R.; Velamakanni, A.; Jung, I.; Tutuc, E.; et al. Large-area synthesis of high-quality and uniform graphene films on copper foils. *Science* **2009**, *324*, 1312–1314.

[6] Kellar, J. A.; Alaboson, J. M. P.; Wang, Q. H.; Hersam, M. C. Identifying and characterizing epitaxial graphene domains on partially graphitized SiC(0001) surfaces using scanning probe microscopy. *Appl. Phys. Lett.* **2010**, *96*, 143103.

[7] Berger, C.; Song, Z. M.; Li, X. B.; Wu, X. S.; Brown, N.; Naud, C.; Mayou, D.; Li, T. B.; Hass, J.; Marchenkov, A. N.; et al. Electronic confinement and coherence in patterned epitaxial graphene. *Science* **2006**, *312*, 1191–1196.

[8] Mao, J. H.; Zhang, H. G.; Jiang, Y. H.; Pan, Y.; Gao, M.; Xiao, W. D.; Gao, H. J. Tunability of supramolecular kagome lattices of magnetic phthalocyanines using graphene-based moire patterns as templates. *J. Am. Chem. Soc.* **2009**, *131*, 14136–14137.

[9] Roos, M.; Kunzel, D.; Uhl, B.; Huang, H. H.; Alves, O. B.; Hoster, H. E.; Gross, A.; Behm, R. J. Hierarchical interactions and their influence upon the adsorption of organic molecules on a graphene film. *J. Am. Chem. Soc.* **2011**, *133*, 9208–9211.

[10] Zhang, H. G.; Sun, J. T.; Low, T.; Zhang, L. Z.; Pan, Y.; Liu, Q.; Mao, J. H.; Zhou, H. T.; Guo, H. M.; Du, S. X.; et al. Assembly of iron phthalocyanine and pentacene molecules on a graphene monolayer grown on Ru(0001). *Phys. Rev. B* **2011**, *84*, 245436.

[11] Li, G.; Zhou, H. T.; Pan, L. D.; Zhang, Y.; Mao, J. H.; Zou, Q.; Guo, H. M.; Wang, Y. L.; Du, S. X.; Gao, H. J. Self-assembly of C_{60} monolayer on epitaxially-grown, nanostructured graphene on Ru(0001) surface. *Appl. Phys. Lett.* **2012**, *100*, 013304.

[12] Zhang, H. G.; Xiao, W. D.; Mao, J. H.; Zhou, H. T.; Li, G.; Zhang, Y.; Liu, L. W.; Du, S. X.; Gao, H. J. Host–guest superstructures on graphene-based kagome lattice. *J. Phys. Chem. C* **2012**, *116*, 11091–11095.

[13] Wang, Q. H.; Hersam, M. C. Room-temperature molecular-resolution characterization of self-assembled organic monolayers on epitaxial graphene. *Nat. Chem.* **2009**, *1*, 206–211.

[14] Wang, Q. H.; Hersam, M. C. Nanofabrication of heteromolecular organic nanostructures on epitaxial graphene via room temperature feedback-controlled lithography. *Nano Lett.* **2011**, *11*, 589–593.

[15] Barja, S.; Garnica, M.; Hinarejos, J. J.; de Parga, A. L. V.; Martin, N.; Miranda, R. Self-organization of electron acceptor molecules on graphene. *Chem. Commun.* **2010**, *46*, 8198–8200.

[16] Huang, H.; Chen, S.; Gao, X. Y.; Chen, W.; Wee, A. T. S. Structural and electronic properties of PTCDA thin films on epitaxial graphene. *ACS Nano* **2009**, *3*, 3431–3436.

[17] Wang, X.; Zhi, L. J.; Mullen, K. Transparent, conductive graphene electrodes for dye-sensitized solar cells. *Nano Lett.* **2008**, *8*, 323–327.

[18] Liu, Z. F.; Liu, Q.; Huang, Y.; Ma, Y. F.; Yin, S. G.; Zhang, X. Y.; Sun, W.; Chen, Y. S. Organic photovoltaic devices based on a novel acceptor material: Graphene. *Adv. Mater.* **2008**, *20*, 3924–3930.

[19] Liu, H. W.; Al-Mahboob, A.; Fujikawa, Y.; Fukui, N.; Hitosugi, T.; Hashizume, T.; Xue, Q. K.; Sakurai, T. Pentacene growth on graphite investigated by low-energy electron microscope. *J. Cryst. Growth* **2010**, *312*, 967–970.

[20] Schroeder, P. G.; France, C. B.; Park, J. B.; Parkinson, B. A. Energy level alignment and two-dimensional structure of pentacene on Au(111) surfaces. *J. Appl. Phys.* **2002**, *91*, 3010–3014.

[21] France, C. B.; Schroeder, P. G.; Forsythe, J. C.; Parkinson, B. A. Scanning tunneling microscopy study of the coverage-dependent structures of pentacene on Au(111). *Langmuir* **2003**, *19*, 1274–1281.

[22] Shi, C.; Wei, C.; Han, H.; Gao, X. Y.; Qi, D. C.; Wang, Y. Z.; Wee, A. T. S. Template-directed molecular assembly on silicon carbide nanomesh: Comparison between CuPc and pentacene. *ACS Nano* **2010**, *4*, 849–854.

[23] Gao, H. J.; Gao, L. Scanning tunneling microscopy of functional nanostructures on solid surfaces: Manipulation, self-assembly, and applications. *Prog. Surf. Sci.* **2010**, *85*, 28–91.

[24] Yoo, S.; Domercq, B.; Kippelen, B. Efficient thin-film organic solar cells based on pentacene/C-60 heterojunctions. *Appl. Phys. Lett.* **2004**, *85*, 5427–5429.

[25] Rao, A.; Wilson, M. W. B.; Hodgkiss, J. M.; Albert-Seifried, S.; Bassler, H.; Friend, R. H. Exciton fission and charge generation via triplet excitons in pentacene/C(60) bilayers. *J. Am. Chem. Soc.* **2010**, *132*, 12698–12703.

[26] Vanderbilt, D. Soft self-consistent pseudopotentials in a generalized eigenvalue formalism. *Phys. Rev. B* **1990**, *41*, 7892–7895.

[27] Kresse, G.; Furthmuller, J. Efficient iterative schemes for *ab initio* total-energy calculations using a plane-wave basis set. *Phys. Rev. B* **1996**, *54*, 11169–11186.

[28] Perdew, J. P.; Burke, K.; Ernzerhof, M. Generalized gradient approximation made simple. *Phys. Rev. Lett.* **1996**, *77*, 3865–3868.

[29] Grimme, S. Semiempirical GGA-type density functional constructed with a long-range dispersion correction. *J. Comput. Chem.* **2006**, *27*, 1787–1799.

[30] Bucko, T.; Hafner, J.; Lebegue, S.; Angyan, J. G. Improved description of the structure of molecular and layered crystals: *Ab initio* DFT calculations with van der Waals corrections. *J. Phys. Chem. A* **2010**, *114*, 11814–11824.

[31] Lu, J.; Yeo, P. S. E.; Zheng, Y.; Yang, Z. Y.; Bao, Q. L.; Gan, C. K.; Loh, K. P. Using the graphene moiré pattern for the trapping of C_{60} and homoepitaxy of graphene. *ACS nano* **2012**, *6*, 944–950.

[32] Gotzen, J.; Kafer, D.; Woll, C.; Witte, G. Growth and structure of pentacene films on graphite: Weak adhesion as a key for epitaxial film growth. *Phys. Rev. B* **2010**, *81*, 085440.

[33] Zhou, H. T.; Mao, J. H.; Li, G.; Wang, Y. L.; Feng, X. L.; Du, S. X.; Mullen, K.; Gao, H. J. Direct imaging of intrinsic molecular orbitals using two-dimensional, epitaxially-grown, nanostructured graphene for study of single molecule and interactions. *Appl. Phys. Lett.* **2011**, *99*, 153101.

[34] Barth, J. V.; Costantini, G.; Kern, K. Engineering atomic and molecular nanostructures at surfaces. *Nature* **2005**, *437*, 671–679.

[35] Xiao, W. D.; Feng, X. L.; Ruffieux, P.; Groning, O.; Mullen, K.; Fasel, R. Self-assembly of chiral molecular honeycomb networks on Au(111). *J. Am. Chem. Soc.* **2008**, *130*, 8910–8912.

[36] Palma, C. A.; Bjork, J.; Bonini, M.; Dyer, M. S.; Llanes-Pallas, A.; Bonifazi, D.; Persson, M.; Samori, P. Tailoring bicomponent supramolecular nanoporous networks: Phase segregation, polymorphism, and glasses at the solid–liquid interface. *J. Am. Chem. Soc.* **2009**, *131*, 13062–13071.